Research Square

Preprints are preliminary reports that have not undergone peer review.
They should not be considered conclusive, used to inform clinical practice,
or referenced by the media as validated information.

Limited climate influence on atmospheric blocking in event-based simulations

Wenqin Zhuo
Yunnan International Joint Laboratory of Monsoon and Extreme Climate Disasters, Department of Atmospheric Sciences, Yunnan University, Kunming, China.
Antonio Sánchez-Benítez
Alfred Wegener Institute Helmholtz-Center for Polar and Marine Research, Bremerhaven, Germany
Marylou Athanase
Alfred Wegener Institute Helmholtz-Center for Polar and Marine Research, Bremerhaven, Germany
Wen Chen
chenwen-dq@ynu.edu.cn

Yunnan International Joint Laboratory of Monsoon and Extreme Climate Disasters, Department of Atmospheric Sciences, Yunnan University, Kunming, China.
Thomas Jung
Alfred Wegener Institute Helmholtz-Center for Polar and Marine Research, Bremerhaven, Germany
Helge F. Goessling
Alfred Wegener Institute Helmholtz-Center for Polar and Marine Research, Bremerhaven, Germany

Research Article

Keywords:

Posted Date: November 27th, 2026

DOI: https://doi.org/10.21203/rs.3.rs-11877228/v1

License: This work is licensed under a Creative Commons Attribution 4.0 International License.
Read Full License

Additional Declarations: The authors declare no competing interests.

Limited climate influence on atmospheric blocking in event-based simulations

Wenqin Zhuo[1,2], Antonio Sánchez-Benítez[2], Marylou Athanase[2], Wen Chen[1,4*], Thomas Jung[2,3], Helge F. Goessling[2]

[1]Yunnan International Joint Laboratory of Monsoon and Extreme Climate Disasters, Department of Atmospheric Sciences, Yunnan University, Kunming, China.

[2]Alfred Wegener Institute Helmholtz-Center for Polar and Marine Research, Bremerhaven, Germany

[3]Institute for Environmental Physics, University of Bremen, Bremen, Germany

[4] Southwest United Graduate School, Kunming, China

*Corresponding author. Email: chenwen-dq@ynu.edu.cn

Abstract

How atmospheric circulation responds to climate change remains a major source of uncertainty for regional extreme-event impacts and adaptation. Event-based storyline approaches replay observed extreme events at different levels of global warming by constraining modelled winds to the observed ones. This isolates how warming changes individual event temperatures, but by design cannot show whether the weather pattern itself would evolve differently. Here we test whether the circulation itself responds to warming during two summer heatwaves and two winter cold spells in Europe, each caused by atmospheric blocking. We constrain the precursor winds only in the lead-up to each event and then let the circulation evolve freely, using ensemble simulations to establish robustness. Conditional on a comparable blocking onset, the subsequent evolution and persistence show little detectable dependence on the background climate state in three of four cases. In one case, however, the block persists substantially longer under 4 °C global warming, dynamically amplifying the associated heatwave. Our results therefore suggest that fixed-circulation storylines can provide useful estimates of the conditional thermodynamic

response, while climate-dependent changes in blocking onset and event-specific changes in subsequent persistence remain important sources of dynamical uncertainty.

Main

With accelerated global warming[1,2], anthropogenic climate change is driving an increase in climate extremes, leading to historically unprecedented cumulative exposure risks over an individual's lifetime[3]. Large uncertainties however remain about how exactly climate change will continue to alter extremes. Event-based storylines have emerged as a widely used approach to determine climate change impacts on specific extreme weather events[4], such as heatwaves[5–7], cold extremes[8,9], precipitation[10,11], droughts[12,13], floods[14,15], etc. Focused on plausibility rather than probability[4,16,17], event-based storylines enable the exploration of alternative versions of observed historical events, thereby also making climate change tangible.

Wind-nudging experiments, which constrain the large-scale horizontal circulation in model simulations to follow a specific (observed) realization of internal variability instead of a quasi-random trajectory, provide a way to isolate non-dynamical aspects of climate and climate change in models, for example to shed light on climate model biases[18,19]. When used to construct climate-change storylines, the winds are imposed in two or more simulations that exhibit different global warming levels. This enables the exploration of thermodynamic climate change impacts given a specific evolution of circulation patterns, including but not limited to resulting extreme weather[5,19,20]. Compared with traditional probabilistic attribution approaches based on observations and free-running simulations[21], wind-nudged storylines provide high signal-to-noise ratios and make it possible to investigate specific processes in detail[5,20,22], but these advantages come at the prize of neglecting possible climate change impacts on the frequency and character of relevant circulation patterns. Given the growing usage of wind-nudged storylines for extreme-event attribution, projection and the potentially important role of atmospheric circulation changes in shaping future extreme events[23], it is essential to scrutinize this method's underlying assumption and to understand how circulation patterns associated with extreme weather respond to climate change.

High-impact extreme weather events in the mid-latitudes are often associated with persistent large-scale circulation anomalies[24,25]. Among them, atmospheric blocking represents one of the most prominent and highly anomalous patterns[26–28]and can result in extreme heatwaves[29,30] and cold spells[31,32]. As a nonlinear circulation system strongly influenced by internal atmospheric variability[33], it is complicated to determine the effects of climate change on individual blocking events and their associated weather extremes in conventional model simulations[26]. Here, we extend the event-based storyline framework by combining spectral wind-nudging experiments with subsequent freely evolving initial-condition ensembles inspired by ensemble boosting[6,34]. Ensemble boosting generates large ensembles of physically plausible extreme events by introducing small perturbations to initial conditions, applied days to weeks before the peak, thereby sampling large ensembles that enable the exploration of even more extreme outcomes. The ensemble boosting approach has been effectively used to produce large samples of heatwave storylines[6,34,35]. We perform similar experiments but focus on how the atmospheric dynamics of extreme events respond to a changed background climate, specifically exploring blocking events associated with two summer heatwaves and two winter cold extremes over Europe. Wind-nudged simulations are first conducted across pre-industrial (PI), present-day (PD), and +4°C global-mean surface temperature climates to precondition the blocking onset, thereby isolating the thermodynamic impact of climate change on the preconditioned model states[5]. Initial-state perturbation ensembles of simulations are continued from the preconditioned states without nudging, allowing the blocking circulation to evolve freely while sampling uncertainty arising from chaotic error growth. Comparing these simulations across different climate backgrounds enables us to assess how the fast dynamics of specific blocking events and their impacts on surface extreme conditions respond to climate change.

Dynamical response of blocking-related extremes to climate warming

We simulate four blocking events associated with extreme weather events in Europe: the 2018 July heatwave over northwestern Europe (Fig. 1b), which triggered severe wildfires across Scandinavia[36]; the 2019 southwestern European heatwave (Fig. 1e), which broke the record of the 2003 heatwave in France[37]; and two winter cold outbreaks of 2015/2016 (Fig. 1h) and 2018 (Fig. 1k) in eastern Europe. Wind-nudged simulations are conducted ahead of each case

(Supplementary Fig. 1), with atmospheric circulation constrained toward ERA5 to generate highly consistent blocking preconditions across all events and climate scenarios. In each case the nudging is stopped around the time of the blocking onset, allowing the model to evolve freely over the course of event (Fig.1) so that the fast dynamics of the blocks can respond to the climate background state. The time of transition from wind-nudged to freely evolving dynamics was tested and determined such that the lead time and thus the dynamical freedom is maximized while the blocking event is still reasonably well reproduced (forecast) in present-day climate conditions. Ensembles of 25 free-running simulations with perturbed initial conditions, hereafter called nudging-stopped simulations, are performed to sample the internal variability of the blocking evolution arising from chaotic error growth.

In the traditional event-based storyline approach with continuous wind-nudging, temperature differences between climates under fixed large-scale circulation are interpreted as thermodynamic response. Here, in contrast, the nudging-stopped simulations entail freely evolving blocking dynamics. By comparing the difference between the 4°C and PD climates in the continuously-nudged and the nudging-stopped simulations, we can quantify how changes in blocking evolution associated with a fast dynamical response to the background climate state further modify the associated surface temperature response (Fig. 2). Overall, despite the discontinued nudging, the subsequent evolution of all blocking events is still reasonably well reproduced, not only in the present-day climate but across all climate states (Figs. 1a, d, g, j; Supplementary Figs. 2-5), indicating a sufficient degree of predictability of these events.

In the 2018 summer heatwave case, the blocking persists longer in the 4°C warmer climate, accompanied by a stronger and more prolonged heatwave over Scandinavia (Fig. 1c, Supplementary Fig.2, Supplementary Fig.6a). Accordingly, the heatwave becomes even more intense in the 4°C warmer climate (Fig. 1c), in particular during its later phase. Relative to the respective background climatology, that is, with the background warming removed, the regional-mean warm anomaly reaches up to +8°C and remains above +5°C until August 4th in the 4°C warmer climate, compared to peaks between +6°C and +7°C and warm anomalies around 3°C on August 4th in the two colder climate states (Supplementary Fig. 6a). Examining the temperature difference between the present-day and the +4°C simulations (Fig. 2a) reveals that the dynamically enhanced warming during the later stage of the event substantially exceeds the

thermodynamics-only response found in the nudged simulations, with the warming in the nudging-stopped simulations (up to +8°C) reaching nearly twice the magnitude of the thermodynamics-only warming in the continuously nudged simulations (around +4°C). This indicates a pronounced dynamical amplification of the 2018 heatwave, further detailed in the following section. However, such behavior is not found across the other events.

In the 2019 heatwave case, the blocking is located further south than in the 2018 case, and it is generally characterized by weaker intensity and a smaller spatial extent (Fig. 1d). In the nudging-stopped simulations, the gradual decline of the blocking amplitude is reasonably well reproduced (Fig. 1d), yet the second temperature peak around July 1st is less pronounced and delayed compared to ERA5 and the nudged simulations (Fig. 1f). Regarding the dynamical response to the climate background state, the blocking peak around June 29th is slightly weaker in the +4°C and PD climates compared to the PI climate, with the opposite being true thereafter, between June 30th and July 2nd. The climate-state driven dynamical response of 2m-temperature is similarly weak (Supplementary Fig. 6b). In contrast to the 2018 case, the changed dynamical conditions lead to a dampened warming in the 4 ºC warmer climate compared to the PD climate around June 30th / July 1st by about half a degree (Fig. 2b). This second case with a much weaker dynamical response to the climate background already suggests that the response of summer blocking dynamics to climate warming is event-specific rather than following a general pattern.

In the 2015/16 winter case, which is the strongest blocking event among the four cases, the blocking exhibits an even higher amplitude and longer duration across all climates compared to ERA5 in the nudging-stopped simulations (Fig. 1g). The ensemble spread of blocking intensity increases during the later stage of the event, indicating limited predictability of how long the block persists (Fig. 1g, Fig. 2c, Supplementary Fig. 6c). Nevertheless, the simulation ensemble still encloses the observed ERA5 evolution of the blocking, suggesting that the simulations are suitable for assessing the dynamical response to the climate background. Overall, as expected, the intensity of the cold outbreak decreases with the climate warming level (Fig.1g, Supplementary Fig. 4). During the later stage of the event, 2m-temperature is slightly colder in the nudging-stopped simulations than in the nudged simulations across all climate scenarios (Fig.1i, Supplementary Fig. 6c). This is consistent with the on average longer prevailing

blocking conditions in the nudging-stopped simulations causing longer-prevailing cold anomalies. However, there is no clear dependence of the blocking intensity and the associated 2m-temperature on the background climate state (Fig. 2c), suggesting no clear fast dynamical response of an event like this one to the degree of climate warming.

A similarly weak dynamical response is found in the 2018 winter case, although in contrast to the previous case the simulated blocking intensity is slightly weaker than in ERA5 in the nudging-stopped simulations (Fig. 1j). Among the climate scenarios, the blocking strength increases slightly from the preindustrial to PD and further to the 4°C climate, similar to the 2018 summer case, but with a weaker sensitivity to climate warming. Correspondingly, 2m-temperature in the 4° C and PD climates is slightly higher in the nudging-stopped simulations than in the nudged experiments, but the overall differences among climate scenarios remain modest (Fig. 1l). Most importantly, no evident modification of the temperature response by fast dynamics is identified in this case (Fig. 2d).

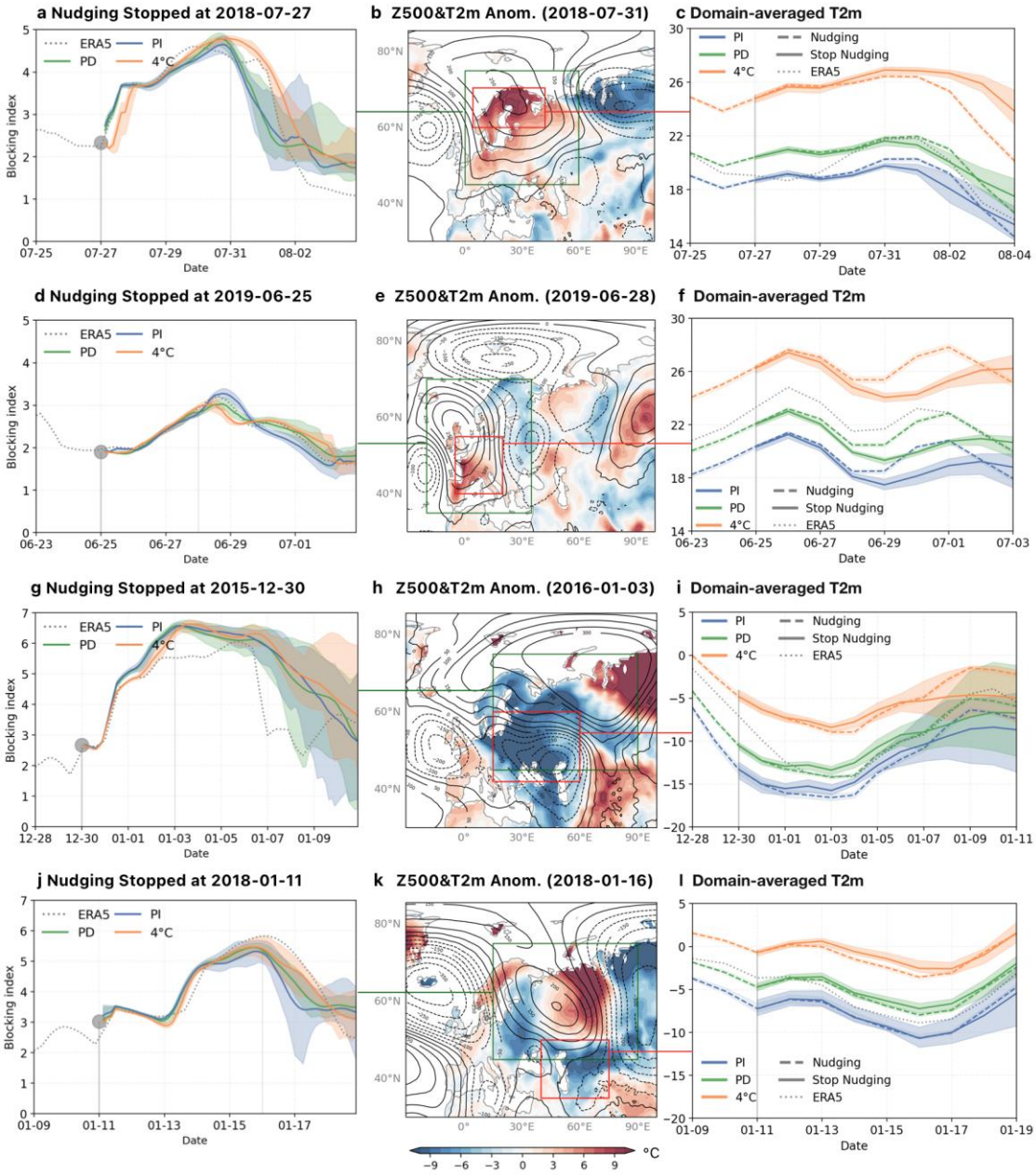

Fig. 1 Blocking intensity and temperature response in nudging-stopped storyline simulations. a,d,g,j Time series of blocking index in nudging-stopped simulations. The grey dashed line shows the ERA5 blocking index; colored lines and shadings indicate the ensemble mean and range across the boosted 25-member nudging-stopped ensembles in different climates. The grey vertical line with a dot marks the date when nudging is stopped, and the date of the peak day of the event is marked by another grey vertical line. **b,e,h,k** Maps of 2m-temperature (T2m; unit:°C) and 500-hPa geopotential height (Z500; unit: gpm) anomalies on the event peak day (second grey vertical line in the left column). The green rectangle indicates the region used

to determine the blocking center maximum, and the red rectangle indicates the domain used to calculate the T2m index. **c,f,i,l** Time series of domain-averaged T2m (unit:°C) in different climates. Colored dashed (solid) lines and shading indicate the continuously nudged (nudging-stopped) simulations, and the grey dashed line indicates ERA5. The grey vertical line marks the date when nudging stops.

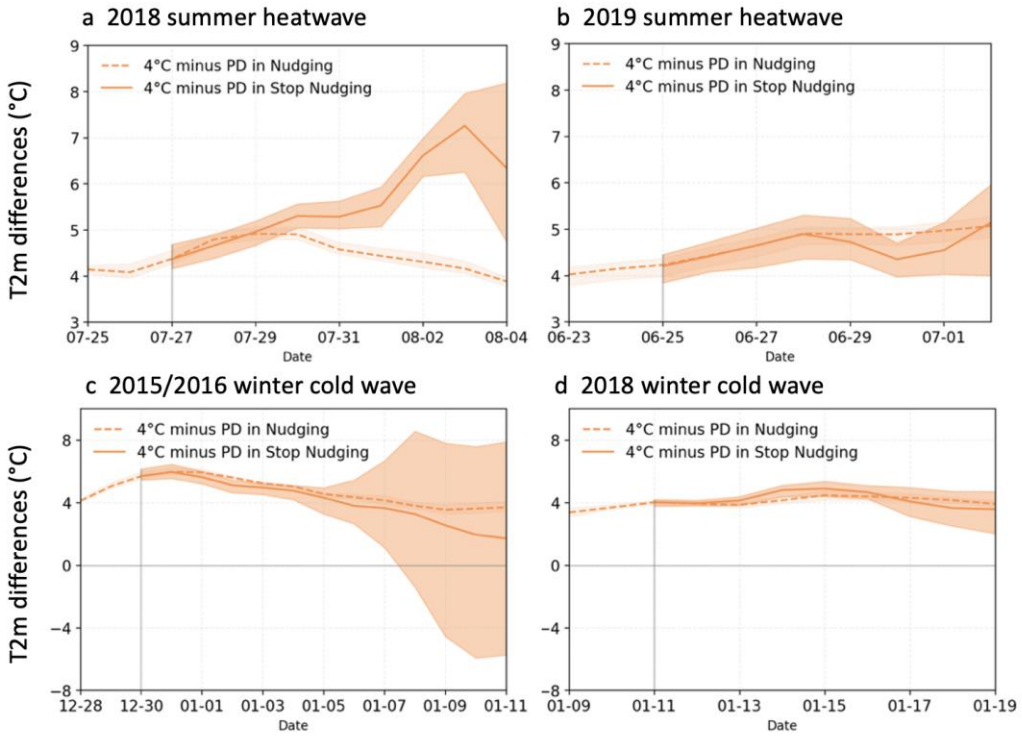

Fig. 2 Temperature response due to changing blocking dynamics. a-d Difference in T2m between the 4°C and PD climates for the continued-nudging (dashed line) and nudging-stopped (solid line) experiments. Shading spans the range across ensemble members. The grey vertical line marks the date when the nudging stops.

Dynamical response and warming amplification of the 2018 summer heat wave

The 2018 summer heatwave over northwestern Europe was associated with the driest conditions in over 35 years[38], causing widespread societal impacts and attracting considerable research attention[30,39,40]. Among the four blocking cases examined in this work, this event is unique in exhibiting strong additional warming amplification by a clear dynamical response.

In the nudging-stopped simulation in PD climate, the heatwave reaches its peak around 31 July / 1 August (Fig. 3c, Fig. 1c, Supplementary Fig. 2), with the warm center located over northern Scandinavia and rapidly declining temperatures thereafter. In contrast, in the 4°C warmer climate, the heatwave persists until 3 August 2018 (Fig. 3j), with extreme heat affecting nearly the entire Scandinavian region and cooling setting in only around 4 August. To further illustrate the spatial distribution of the thermodynamic and dynamic warming shown in Fig. 2a, Fig.3k-t presents the evolution of how the spatial pattern of 2m-temperature climate-change anomalies differs between the nudging-stopped (k-o) and the continuously nudged (p-t) simulations. During the early stage of the event, the spatial warming patterns are very similar (Fig. 2a; Fig. 3k, l, p, g), which is not surprising given that any dynamical differences require time to develop. Subsequently, however, the purely thermodynamic warming amplification in the continuously nudged simulations gradually weakens and disappears (Fig. 2a; Fig. 3r, s, t), whereas the warming amplification in the nudging-stopped simulations continues to intensify (Fig. 2a; Fig. 3m, n, o), with its maximum centered over northern Scandinavia around 2 August and then shifting eastward. This suggests that changes in the dynamics of a blocking event such as this one can prolong and intensify associated extreme heat. This stands in contrast to the other three cases, which exhibit only weak dynamic warming amplification owing to their limited dynamic response of the blocking circulation (Fig. 2b-d; Supplementary Figs. 7–9).

The physical mechanisms underlying the enhanced blocking persistence in the warmer climate, and why they operate in one but not the other three cases, cannot be uniquely identified from the present experiments, but several pathways are plausible. The maintenance and decay of blocking depend on interactions between the block, the background flow, and transient synoptic eddies, including their associated vorticity and potential-vorticity (PV) forcing, Rossby-wave propagation and wave breaking[26,41,42], as well as the background meridional PV gradient prior to blocking onset[33]. Moist diabatic processes can also contribute to block amplification and maintenance through latent heating in ascending airstreams and the associated generation and transport of low-PV air into the upper-tropospheric ridge[43,44]. Besides, surface heating associated with heatwaves can induce diabatic heating in the mid-troposphere[45], a feedback that might become more pronounced under 4°C warming and potentially affect the subsequent evolution of a blocking system.

These mechanisms are particularly relevant in the context of the present experimental design. Prior to release, spectral nudging constrains not only the blocking circulation but also its planetary-wave environment and, during the strong-nudging phase, part of the synoptic-scale circulation. In contrast, thermodynamic properties such as temperature, moisture and stability remain climate-state dependent. Once nudging is stopped, climate-dependent differences in diabatic processes and synoptic evolution can therefore progressively modify eddy and PV forcing, Rossby-wave evolution and ultimately the persistence of the initially similar blocking circulation.

The delayed separation between the PD and +4°C simulations in the 2018 case is consistent with such a progressive adjustment, although the present analysis does not allow the responsible mechanism to be identified. More generally, the event-specific response may reflect differences in the stability of an initially similar blocking state within different background climates. If an event is close to a transition between persistence and decay, relatively small climate-dependent changes in eddy forcing, diabatic processes or background-flow characteristics could lead to substantially different subsequent trajectories. This provides one possible interpretation of why a pronounced persistence response emerges for the 2018 event but not the other cases considered here.

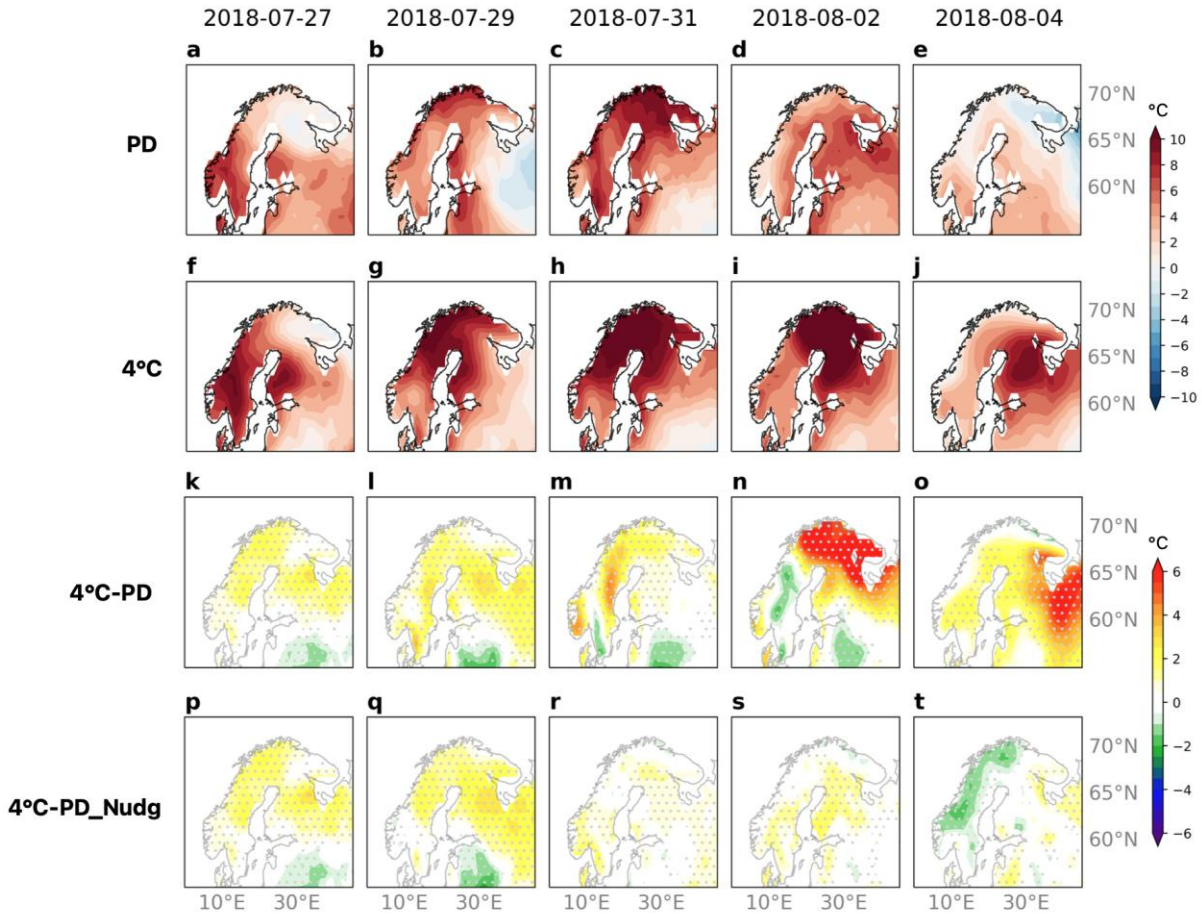

Fig. 3 Spatial patterns of surface warming amplification of the 2018 summer heat wave. a-e Ensemble-mean 2m-temperature anomalies (relative to PD climatology) of the 2018 summer heat wave in the PD climate in nudging-stopped simulations. **f-j** Same as a-e but for the 4°C climate (relative to +4°C climatology). **k-o** Warming amplification (difference in 2m-temperature anomaly between 4°C and PD climate) in nudging-stopped simulations. Grey dots denote regions where the difference is significant at the 95% level based on local Student's *t* tests. **p-t** same as in **k-o** but based on continuously nudged simulations.

Summary and discussion

The spectrally wind-nudged storyline approach provides an effective framework for assessing the thermodynamic influence of anthropogenic climate change on extreme events under fixed large-scale circulation conditions[4,5,8,10,16]. This approach shares a key assumption with other

conditional attribution approaches[46], such as pseudo-global-warming simulations[47] and circulation-analogue methods[48] that the evolution of large-scale circulation patterns during the event is not affected by the thermodynamic climate background. Here, we test this assumption by extending the event-based storyline framework by allowing the circulation to evolve freely after stopping the nudging around the time of the blocking onset. Initial-condition ensembles enable us to sample the internal variability developing through chaotic error growth.

The preceding nudging constrains not only the blocking onset itself but also its larger-scale planetary-wave environment and, particularly during the final strong-nudging phase, part of the synoptic-scale circulation. Consequently, these nudging-stopped experiments do not sample the full climate response of blocking, including potential changes in its precursors and onset dynamics. Instead, they test whether an initially similar dynamical state evolves differently once released in different background climates. This framework therefore provides a targeted assessment of the climate dependence of the subsequent evolution and persistence of specific blocking events to climate change, while also helping to clarify the interpretation and limitations of the original event-based storyline approach where continuous nudging is applied.

The nudging-stopped simulations of four blocking events associated with two summer heatwaves and two winter cold outbreaks are generally able to predict the blocking evolution on timescales of approximately one week with reasonable skill, which is an important prerequisite for our study. Among these cases, only the 2018 Scandinavian summer heatwave exhibits a substantial dynamically induced response, with a more persistent blocking under the 4 °C global warming climate producing additional dynamic surface warming that substantially prolongs the heatwave. For the other three cases, we find little evidence that background warming substantially alters the subsequent short-term evolution of the block, conditional on a comparable blocking onset. These results support useful estimates of the conditional thermodynamic response, while climate-dependent changes in blocking onset and event-specific changes in subsequent persistence remain important sources of dynamical uncertainty.

Our approach and findings complement forecast-based attribution, in which ensemble weather forecasts of the event are run under different climate forcing but are all initialised from the same observed present-day atmosphere[46,49], rather than from a state nudged

within each climate. Such previous forecast attribution studies[49,50] similarly found little change in the large-scale evolution of two heatwave events across climates, in line with our results for three of the four blocking events. In contrast, an event-specific dynamical response, similar to the 2018 blocking prolongation, was identified during storm Eunice over UK[51]: a moister warm conveyor belt enhanced latent heating and vorticity production, intensifying the storm in a warmer climate. We note that they focused on heatwaves and a storm, rather than specifically on blocking dynamics. Nevertheless, both our findings and this previous work[51] thus suggest that, conditional on a comparable initial state, background warming mainly does act through the thermodynamic response, while fast dynamical responses may modulate the evolution of specific events.

It remains important to further explore the role of dynamical changes for extreme-event attribution, including analyses of more events and event types in different regions and of slower dynamics that are not captured by our method. Yet our results provide strong evidence that dynamical effects do not fundamentally undermine event-based storyline approaches based on fixed-circulation simulations. The wind-nudged storyline approach therefore appears broadly applicable to estimate first-order climate change impacts on individual extreme events, whilst keeping in mind that fast dynamical responses may modulate certain high-impact extremes in warmer climates and that slower dynamics remain to be explored.

Methods

Wind-nudged simulations and determination of initial times

The simulations are conducted using AWI-CM-1-1-MR[52], a global, coupled climate model which contributed to the Coupled Model Intercomparison Project Phase 6 (CMIP6)[53]. It employs the ECHAM6.3.04p1 atmospheric model[54,55] and the Finite Element Sea Ice–Ocean Model (FESOM) v.1.4[54]. In the continued-nudging simulations, vorticity and divergence between 700 and 100 hPa are first softly nudged toward ERA5 reanalysis from five free-running CMIP6 members, using a 24-h relaxation timescale and applied to zonal wavenumbers up to 20^5. The model states obtained from the nudging simulations are used as initial conditions for the following free-running forecast-like simulations to cover the evolution of the respective blocking events. Ideally, the initialization time should be early enough to allow maximum dynamical

freedom for the atmospheric circulation to adjust to the imposed background climate state, while still providing sufficient forecast skill to realistically reproduce the subsequent evolution of the blocking event.

Preliminary tests of soft nudging alone show insufficiently accurate initial conditions for the blocking events to be forecast reasonably well in PD simulations. We therefore introduced a short period of strong nudging following the preceding soft-nudging phase, using a 1-h relaxation timescale and extending the nudging to all wavenumbers up to 127. This substantially reduced the ensemble spread and brought the simulated circulation closer to ERA5, thereby providing more accurate initial conditions for the subsequent free-running simulations. The duration of strong nudging was determined separately for each event through day-by-day sensitivity tests with different initialization times, based on the subsequent evolution of the blocking index.

Accordingly, for the 2018 heatwave case, soft nudging was applied until 30 June 2018, followed by strong nudging until 26 July 2018. For the 2019 heatwave case, soft nudging continued until 31 May 2019 and strong nudging until 24 June 2019. For the 2015/2016 cold-wave case, soft nudging continued until 30 November 2015 and strong nudging until 29 December 2015. Finally, for the 2018 winter case, soft nudging continued until 31 December 2017 and strong nudging until 10 January 2018. The same procedure was applied to the counterfactual climates, using the corresponding model years for each climate state. The period 2017–2021 in the PD climate corresponds to model years 2093–2097 in the +4 °C climate and 1851–1855 in the PI climate, and the period 2014–2017 corresponds to model years 2090–2093 (+4 °C) and 1854–1857 (PI), respectively.

Additional initial-state perturbations

After nudging is stopped, the original five-member ensembles are expanded to twenty-five members by applying additional perturbations in order to better sample the internal variability arising from chaotic error growth. In order to maintain spatio-temporal and inter-variable consistency of the perturbations, including awareness of the time-dependent variance structure, the perturbations are derived from the deviation of each of the five original ensemble members

from the ensemble mean. The perturbations are added to each of the other original members to obtain the perturbed states:

$$E_{n,p}^{P} = E_n + \delta\left(E_p - E_{mean}\right), \qquad \mathrm{n} \in \{1, \ldots, 5\}, \;\; p \neq n \tag{3}$$

where E_n is the n-th original (base) member, E_p is the p-th original member, and E_{mean} is the ensemble mean of all five original ensemble members. δ is a scaling factor controlling the perturbation amplitude. Testing different scaling factors, we found that δ=1 produces a similar error growth between pairs of perturbed members sharing the same base member n, compared to pairs of different base members (Supplementary Fig. 10), which we consider to be a plausible choice. Perturbations are applied to 35 atmospheric variables, as listed in Supplementary Table 1, which essentially constitute the whole atmospheric state. Note that, in principle, there are fewer prognostic atmospheric variables, but additional derivatives and information from the previous timestep are required due to the numerical discretization. Additional soil and ocean state variables are left unperturbed but inherit the differences from the base ensemble members.

Definition of blocking index

We compute a blocking index (BI) based on the methodology of previous work[33,59]:

$$BI = 100.0\left[\frac{MZ}{RC} - 1.0\right] \tag{1}$$

$$RC = \frac{\frac{Z_u + MZ}{2} + \frac{Z_d + MZ}{2}}{2} \tag{2}$$

In (1), MZ is the maximum 500-hPa geopotential height in the closed anticyclone region. Following previous methodology[57], with a slight modification, we define Z_u and Z_d in (2) as the minimum Z500 values within a 60° longitude range upstream and downstream of the maximum location, respectively.

In this way, the definition of BI takes into account both the blocking intensity measured in its center and the level of the surrounding low vortex or troughs. The minimum value for BI is 0, with higher values indicating stronger blocking events. As the blocking index is calculated over

the full duration of each case, the movement of the blocking center must be taken into account. We therefore define a reference region within which the MZ is identified, as indicated by the green rectangles in Fig.1b (0°E – 60°E, 45°N– 75°N), Fig. 1e (−20°E– 35°E, 45°N– 75°N), Fig.1h (15°E – 90°E, 45°N– 75°N), Fig.1k (15°E – 90°E, 45°N– 75°N), which always encompasses the maximum center of each specific blocking event as it evolves. As an auxiliary criterion to avoid multiple local maxima even when no well-defined block is present anymore, the MZ is identified only within the region of positive Z500 anomalies, ensuring a physically consistent location.

Anomalies and climatology

For the present-day (PD) climate, the climatology spans the period 1985–2014 and is calculated as the ensemble mean of the five free-running historical CMIP6 simulations of the same model AWI-CM-1-1-MR, with a 31-day running mean applied to obtain a smooth seasonal cycle, here referred to as $clim_{PD}$. Anomalies in the PD climate are obtained by subtracting $clim_{PD}$. For the +4°C and preindustrial (PI) climates, the climatologies $clim_{4K_adj}$ and $clim_{PI_adj}$ are obtained by adjusting $clim_{PD}$ with the climate-change signals derived from the wind-nudged simulations:

$$clim_{4K_adj} = clim_{PD} + \left(clim_{nudg_4K} - clim_{nudg_PD}\right) \quad (4)$$

$$clim_{PI_adj} = clim_{PD} + \left(clim_{nudg_PI} - clim_{nudg_PD}\right) \quad (5)$$

where $clim_{nudg_PI}$, $clim_{nudg_PD}$, and $clim_{nudg_4K}$ denote the ensemble-mean climatologies of the softly nudged simulations for the period 2017-2021 in the different climate states, all smoothed using a 14-day running mean to obtain a less noisy seasonal cycle. Accordingly, the anomalies in the PI and 4°C climates are determined by subtracting $clim_{PI_adj}$ and $clim_{4K_adj}$, respectively.

Reanalysis data

Beside the wind data for the nudging, we also use daily 2m-temperature (T2m) and 500-hPa geopotential height from the ERA5 reanalysis[58] as observation-based reference for comparison with the PD nudged climate simulations.

Data availability and Code availability

Upon publication, the data and code necessary to reproduce all figures presented in the manuscript will be made available as open-access resources in citable Zenodo archives.

Acknowledgements

This work was supported by the Helmholtz Research Field Earth & Environment for the Innovation Pool Projects SCENIC and ACTUATE, the Postdoctoral Fellowship Program of China Postdoctoral Science Foundation under Grant Number GZC20250199, the Yunnan Provincial Science and Technology Department (Award numbers 202505AB350001, 202403AP140009), and by the European Union's Horizon Europe research and innovation programme under Grant Agreement No. 101295874 (SUNRISE). All simulations were performed at the German Climate Computing Center (DKRZ) using ESM Tools[59] and resources from the ba1264 project.

Reference

1. Goessling, H. F., Rackow, T. & Jung, T. Recent global temperature surge intensified by record-low planetary albedo. *Science (New York, N.Y.)* **387**, 68–73 (2025).
2. Foster, G. & Rahmstorf, S. Global Warming Has Accelerated Significantly. *Geophysical Research Letters* **53**, e2025GL118804 (2026).
3. Bevacqua, E., Schleussner, C.-F. & Zscheischler, J. A year above 1.5 °C signals that Earth is most probably within the 20-year period that will reach the Paris Agreement limit. *Nat. Clim. Chang.* **15**, 262–265 (2025).
4. Shepherd, T. G. *et al.* Storylines: an alternative approach to representing uncertainty in physical aspects of climate change. *Climatic Change* **151**, 555–571 (2018).

5. Sánchez Benítez, A., Goessling, H., Pithan, F., Semmler, T. & Jung, T. The July 2019 European heatwave in a warmer climate: Storyline scenarios with a coupled model using spectral nudging. *Journal of Climate* 1–51 (2022) doi:10.1175/jcli-d-21-0573.1.

6. Fischer, E. M. *et al.* Storylines for unprecedented heatwaves based on ensemble boosting. *Nature Communications* **14**, 1–11 (2023).

7. Qian, C. *et al.* Rapid attribution of the record-breaking heatwave event in North China in June 2023 and future risks. *Environmental Research Letters* **19**, (2024).

8. Zhuo, W. *et al.* Storylines reveal contrasting thermodynamic effects of climate change on 2020/21 East Asian cold extremes. *npj Climate and Atmospheric Science 2025 8:1* **8**, 1–10 (2025).

9. Sippel, S. *et al.* Could an extremely cold central European winter such as 1963 happen again despite climate change? *Weather and Climate Dynamics* **5**, 943–957 (2024).

10. Athanase, M., Sánchez-Benítez, A., Monfort, E., Jung, T. & Goessling, H. F. How climate change intensified storm Boris' extreme rainfall, revealed by near-real-time storylines. *Communications Earth & Environment 2024 5:1* **5**, 1–5 (2024).

11. Campos, D. A. *et al.* The October 2024 Extreme Precipitation Event over Valencia: Storyline Attribution of the Synoptic-Scale Thermodynamic Drivers. Preprint at https://doi.org/10.5194/egusphere-2025-5929 (2025).

12. Gessner, C., Fischer, E. M., Beyerle, U. & Knutti, R. Multi-year drought storylines for Europe and North America from an iteratively perturbed global climate model. *Weather and Climate Extremes* **38**, 100512 (2022).

13. van Garderen, L. & Mindlin, J. A storyline attribution of the 2011/2012 drought in Southeastern South America. *Weather* **77**, 212–218 (2022).

14. Schaller, N. *et al.* The role of spatial and temporal model resolution in a flood event storyline approach in western Norway. *Weather and Climate Extremes* **29**, 100259 (2020).

15. Wang, J. *et al.* Storyline attribution of human influence on a record-breaking spatially compounding flood-heat event. *Science Advances* **9**, eadi2714 (2023).

16. Wehrli, K., Hauser, M. & Seneviratne, S. I. Storylines of the 2018 Northern Hemisphere heatwave at pre-industrial and higher global warming levels. *Earth System Dynamics* **11**, 855–873 (2020).

17. Sillmann, J. *et al.* Event-Based Storylines to Address Climate Risk. *Earth's Future* **9**, e2020EF001783 (2021).

18. Wehrli, K., Guillod, B. P., Hauser, M., Leclair, M. & Seneviratne, S. I. Assessing the Dynamic Versus Thermodynamic Origin of Climate Model Biases. *Geophysical Research Letters* **45**, 8471–8479 (2018).

19. Pithan, F. *et al.* Nudging allows direct evaluation of coupled climate models with in-situ observations : A case study from the MOSAiC expedition. *EGUsphere* 1–23 (2022).

20. Van Garderen, L., Feser, F. & Shepherd, T. G. A methodology for attributing the role of climate change in extreme events: A global spectrally nudged storyline. *Natural Hazards and Earth System Sciences* **21**, 171–186 (2021).

21. Shepherd, T. G. A Common Framework for Approaches to Extreme Event Attribution. *Current Climate Change Reports* **2**, 28–38 (2016).

22. Athanase, M., Sánchez-Benítez, A., Goessling, H. F., Pithan, F. & Jung, T. Projected amplification of summer marine heatwaves in a warming Northeast Pacific Ocean. *Communications Earth and Environment* **5**, 1–12 (2024).

23. Otto, F. E. L. *et al.* The attribution question. *Nature Clim Change* **6**, 813–816 (2016).

24. Francis, J. A., Skific, N. & Vavrus, S. J. Increased persistence of large-scale circulation regimes over Asia in the era of amplified Arctic warming, past and future. *Sci Rep* **10**, 14953 (2020).

25. Gong, H. *et al.* Teleconnection from Arctic warming suppresses long-term warming in central Eurasia. *Science Advances* https://doi.org/10.1126/sciadv.adq9461 (2025) doi:10.1126/sciadv.adq9461.

26. Woollings, T. *et al.* Blocking and its Response to Climate Change. *Curr Clim Change Rep* **4**, 287–300 (2018).

27. Lupo, A. R. & Smith, P. J. Climatological features of blocking anticyclones in the Northern Hemisphere. *Tellus A* **47**, 439–456 (1995).

28. Hanna, E. *et al.* Influence of high-latitude blocking and the northern stratospheric polar vortex on cold-air outbreaks under Arctic amplification of global warming. *Environmental Research: Climate* **3**, 042004 (2024).

29. Fang, B. & Lu, M. Heatwave and Blocking in the Northeastern Asia: Occurrence, Variability, and Association. *Journal of Geophysical Research: Atmospheres* **125**, e2019JD031627 (2020).

30. Li, M. *et al.* Collaborative impact of the nao and atmospheric blocking on european heatwaves, with a focus on the hot summer of 2018. *Environmental Research Letters* **15**, (2020).

31. Hannaa, E. *et al.* Influence of high-latitude blocking and the northern stratospheric polar vortex on cold-air outbreaks under Arctic amplification of global warming OPEN ACCESS Influence of high-latitude blocking and the northern stratospheric polar vortex on cold-air outb. (2024).

32. Zhuo, W., Yao, Y., Luo, D., Simmonds, I. & Huang, F. Combined impact of the cold vortex and atmospheric blocking on cold outbreaks over East Asia and the potential for short-range prediction of such occurrences. *Environ. Res. Lett.* **17**, 084037 (2022).

33. Luo, D., Zhang, W., Zhong, L. & Dai, A. A nonlinear theory of atmospheric blocking: A potential vorticity gradient view. *Journal of the Atmospheric Sciences* **76**, 2399–2427 (2019).

34. Gessner, C., Fischer, E. M., Beyerle, U. & Knutti, R. Very rare heat extremes: Quantifying and understanding using ensemble reinitialization. *Journal of Climate* **34**, 6619–6634 (2021).

35. Bloin-Wibe, L. *et al.* Estimating return periods for extreme events in climate models through Ensemble Boosting. Preprint at https://doi.org/10.5194/egusphere-2025-525 (2025).

36. Vogel, M. M., Zscheischler, J., Wartenburger, R., Dee, D. & Seneviratne, S. I. Concurrent 2018 Hot Extremes Across Northern Hemisphere Due to Human-Induced Climate Change. *Earth's Future* **7**, 692–703 (2019).

37. Mitchell, D., Kornhuber, K., Huntingford, C. & Uhe, P. The day the 2003 European heatwave record was broken. *The Lancet Planetary Health* **3**, e290–e292 (2019).

38. Rösner, B. *et al.* The long heat wave and drought in Europe in 2018. *Bulletin of the American Meteorological Society* **100**, S222–S223 (2019).

39. Drouard, M., Kornhuber, K. & Woollings, T. Disentangling Dynamic Contributions to Summer 2018 Anomalous Weather Over Europe. *Geophysical Research Letters* **46**, 12537–12546 (2019).

40. Kueh, M. T. & Lin, C. Y. The 2018 summer heatwaves over northwestern Europe and its extended-range prediction. *Scientific Reports 2020 10:1* **10**, 1–18 (2020).

41. Drouard, M. & Woollings, T. Contrasting Mechanisms of Summer Blocking Over Western Eurasia. *Geophysical Research Letters* **45**, 12,040-12,048 (2018).

42. Kautz, L.-A. *et al.* Atmospheric blocking and weather extremes over the Euro-Atlantic sector – a review. *Weather and Climate Dynamics* **3**, 305–336 (2022).

43. Pfahl, S., Schwierz, C., Croci-Maspoli, M., Grams, C. M. & Wernli, H. Importance of latent heat release in ascending air streams for atmospheric blocking. *Nature Geosci* **8**, 610–614 (2015).

44. Steinfeld, D. & Pfahl, S. The role of latent heating in atmospheric blocking dynamics: a global climatology. *Clim Dyn* **53**, 6159–6180 (2019).

45. Zhang, Y. & Boos, W. R. An upper bound for extreme temperatures over midlatitude land. *Proc. Natl. Acad. Sci. U.S.A.* **120**, e2215278120 (2023).

46. Thompson, V., Ermis, S. & Athanase, M. The need for multi-method extreme event attribution. *Weather* **81**, 40–45 (2026).

47. Schär, C., Frei, C., Lüthi, D. & Davies, H. C. Surrogate climate-change scenarios for regional climate models. *Geophysical Research Letters* **23**, 669–672 (1996).

48. Faranda, D. *et al.* ClimaMeter: contextualizing extreme weather in a changing climate. *Weather and Climate Dynamics* **5**, 959–983 (2024).

49. Leach, N. J., Weisheimer, A., Allen, M. R. & Palmer, T. Forecast-based attribution of a winter heatwave within the limit of predictability. *Proceedings of the National Academy of Sciences* **118**, e2112087118 (2021).

50. Leach, N. J. *et al.* Heatwave attribution based on reliable operational weather forecasts. *Nat Commun* **15**, 4530 (2024).

51. Ermis, S., Leach, N. J., Lott, F. C., Sparrow, S. N. & Weisheimer, A. Event attribution of a midlatitude windstorm using ensemble weather forecasts. *Environ. Res.: Climate* **3**, 035001 (2024).

52. Semmler, T. *et al.* Simulations for CMIP6 With the AWI Climate Model AWI-CM-1-1. *Journal of Advances in Modeling Earth Systems* **12**, e2019MS002009 (2020).

53. Eyring, V. *et al.* Overview of the Coupled Model Intercomparison Project Phase 6 (CMIP6) experimental design and organization. *Geoscientific Model Development* **9**, 1937–1958 (2016).

54. Stevens, B. *et al.* Atmospheric component of the MPI-M Earth System Model: ECHAM6. *Journal of Advances in Modeling Earth Systems* **5**, 146–172 (2013).

55. Wang, Q. *et al.* The Finite Element Sea Ice-Ocean Model (FESOM) v.1.4: Formulation of an ocean general circulation model. *Geoscientific Model Development* **7**, 663–693 (2014).

56. Wiedenmann, J. M., Lupo, A. R., Mokhov, I. I. & Tikhonova, E. A. The climatology of blocking anticyclones for the Northern and Southern Hemispheres: Block intensity as a diagnostic. *Journal of Climate* **15**, 3459–3473 (2002).

57. Davini, P., Cagnazzo, C., Gualdi, S. & Navarra, A. Bidimensional diagnostics, variability, and trends of northern hemisphere blocking. *Journal of Climate* **25**, 6496–6509 (2012).

58. Hersbach, H. *et al.* The ERA5 global reanalysis. *Quarterly Journal of the Royal Meteorological Society* **146**, 1999–2049 (2020).

59. Semmler, T. *et al.* AWI AWI-CM1.1MR model output prepared for CMIP6 CMIP historical. (2018) doi:10.22033/ESGF/CMIP6.2686.

Supplementary Files

This is a list of supplementary files associated with this preprint. Click to download.

- Supplementaryfiles.docx